Terrestrial OH nightglow measurements during the Rosetta fly-by

Migliorini, A.[1], (Alessandra.Migliorini@iaps.inaf.it)

Gérard, J.C.[2], (JC.Gerard@ulg.ac.be)

Soret, L.[2], (lauriane.soret@ulg.ac.be)

Piccioni, G.[1], (Giuseppe.Piccioni@iaps.inaf.it)

Capaccioni, F.[1], (Fabrizio.Capaccioni@iaps.inaf.it)

Filacchione, G.[1], (Gianrico.Filacchione@iaps.inaf.it)

Snels, M.[3], (m.snels@isac.cnr.it)

Tosi, F.[1], (Federico.Tosi@iaps.inaf.it)

[1] INAF-IAPS, Istituto di Astrofisica e Planetologia Spaziali, Via del Fosso del Cavaliere, 100, 00133 Rome, Italy

[2] LPAP, Université de Liège, Allée du 6 Août, 17 – Sart Tilman, B-4000 Liège, Belgium

[3] ISAC-CNR, via del Fosso del Cavaliere, 100, 00133 Rome, Italy

Corresponding author: Dr. Alessandra Migliorini,

Address: INAF-IAPS, Via del Fosso del Cavaliere, 100 - I - 00133, Rome, Italy

e-mail: Alessandra.Migliorini@iaps.inaf.it,

Tel: +39-06-45488-560

Fax: +39-06-45488-188

Abstract

We present a study of the terrestrial hydroxyl nightglow emissions observed with the Visible and Infrared Thermal Imaging Spectrometer (VIRTIS) on board the Rosetta mission. During these observations, the OH Δv=1 and 2 sequences were measured simultaneously. This allowed investigating the relative population of the v=1 to 9 vibrational levels by using both sequences. In particular, the relative population of the vibrational level v=1 is determined for the first time from observations. The vibrational population decreases with increasing vibrational quantum number. A good agreement is found with a recent model calculation assuming multi-quantum relaxation for OH(v) quenching by O_2 and single-quantum relaxation for OH(v) by N_2.

1. Introduction

The Meinel bands of hydroxyl are a good proxy to investigate atmospheric properties for the terrestrial planets. These emissions have been extensively used to study the photochemical and dynamical properties of the atmosphere in the Earth's upper mesosphere. Vibrationally excited OH is produced through the Bates-Nicolet mechanism following the chemical reaction [*Bates and Nicolet,* 1950]:

$$H + O_3 \rightarrow OH^{\cdot}(v \leq 9) + O_2 \qquad \text{(a)}$$

which is effective in the Earth, Mars and Venus atmospheres. The reaction involving HO_2 short-lived molecules:

$$O + HO_2 \rightarrow OH^{\cdot}(v \leq 6) + O_2 \qquad \text{(b)}$$

was found to be negligible in the excitation of the Earth's OH Meinel bands with v up to 6 [*Meriwether,* 1989], although its role is still debated, as discussed in *Xu et al.*[2012].

On Earth, the OH airglow layer is located near the mesopause [*Lowe et al.,* 1996*; She and Lowe,* 1998], with a maximum at 87 km and a full width at half maximum (FWHM) of about 8 km [*Baker and Stair,* 1988].

Several studies based on ground- and space-based observations demonstrated that the OH Meinel emission profile is strongly sensitive to the atmospheric temperature and density profiles. Dynamic structures, like tides [*Xu et al.,* 2010*; Zhang et al.,* 1998*; Shepherd et al.,* 1998*; Ward,* 1999*; Zhang and Shepherd,* 1999*; Russell et al.,* 2005*; Liu et al.,* 2008] or planetary waves [*Snively et al.,* 2010*; Gao et al.,* 2010] are found to affect the peak altitude by modulating the OH emission profile. Quenching by atomic oxygen contributes also to the vertical shift observed in the peak altitudes

53 from different Meinel bands [*von Savigny and Lednyts'kyy, 2013*]. Temperature inversions and
54 minor species mixing effects are also responsible for changes in the OH airglow vertical profile
55 [*Melo et al.,* 1999*; von Savigny et al.,* 2012]. Moreover, it has been observed that the emission
56 originating from higher vibrational levels typically occurs at higher altitudes [*von Savigny et al.,*
57 2012]. Ground-based spectroscopy of the OH airglow has also been used to infer the mesospheric
58 temperature at the airglow altitudes [*Zhao et al.,* 2005*; She and Lowe,* 1998].
59 Here we present an analysis of the OH(Δv=1,2) sequences in the Earth's atmosphere, observed
60 with the Visible and Infrared Thermal Imaging Spectrometer (VIRTIS) on board the Rosetta
61 spacecraft, during the Earth fly-by in November 2009, in order to obtain the population distribution
62 of the vibrational levels.
63 The observing geometry has limited the lowest accessible altitude to 87 km, with a vertical
64 resolution on the order of 10 km/pixel at best. Hence we limit our investigation to the altitude range
65 87-105 km, without exploring the vertical dependence of the emission. Moreover, the spectral
66 resolution is not adequate to resolve single ro-vibrational transitions, and the vibrational manifolds
67 are only partly resolved. For this reason, we assume that a Gaussian shape reproduces the emission
68 layer.
69 Our analysis will be compared with previous ground-based and space observations and with
70 model calculations. The method we employ in this analysis presents the advantage of being less
71 sensitive to spurious signals and instrumental artifacts because it uses the Δv=1 and Δv=2 spectra
72 which were simultaneously observed. In addition, spectra observed from space are not affected by
73 telluric absorptions, hence the full OH(Δv=1,2) sequences of emissions can be retrieved without
74 correction for atmospheric extinction.
75 In section 2 the analysis of the VIRTIS/Rosetta spectral data is described, focusing on the
76 terrestrial OH nightglow emission in the infrared. An empirical radiative model of the spectral
77 range where OH(Δv=1,2) emissions occur is described in section 3 with the aim to allow a retrieval

78 of the vibrational populations. In section 4, we discuss the results and compare them with analyses
79 of experimental ground-based observations and theoretical works.
80
81 **2. Data selection**
82
83 Rosetta is the first large-class European mission devoted to the close investigation of small
84 bodies in the Solar System [*Schulz,* 2009]. It was launched on 2nd March 2004 towards the primary
85 target of the mission, comet 67P/Churyumov-Gerasimenko (67P/C-G). The main scientific
86 objectives of the Rosetta mission dealt with the study of the comet 67P/C-G, with special emphasis
87 on its nucleus and coma. Gravity assist maneuvers with the Earth and Mars [*Coradini et al.,* 2010*;*
88 *Migliorini et al.,* 2013] were performed during the ten year-long cruise phase, as well as fly-bys
89 with the main belt asteroids (2867) Steins [*Tosi et al.,* 2010; *Leyrat et al.,* 2011] and (21) Lutetia
90 [*Coradini et al.,* 2011]. The investigation of the planetary airglow emissions is one of the goals
91 foreseen for the mission during the Earth and Mars fly-bys.
92 The VIRTIS instrument [Coradini et al., 2007] includes two spectral channels: (1) the VIRTIS-
93 M mapping spectrometer, with imaging capabilities and a medium spectral resolution and (2) the
94 VIRTIS-H echelle spectrometer, with a higher spectral resolution compared to VIRTIS-M, but
95 without imaging capabilities. VIRTIS-M covers the 0.3–5.1 μm range in 864 spectral bands by
96 means of two co-aligned channels: the Vis/NIR channel, operating from 0.3 to 1.0 μm with a
97 spectral sampling of 2 nm; and the IR channel, from 1.0 to 5.1 μm with a spectral sampling of 9.5
98 nm; the spectral resolution is of the order of 3 nm and 20 nm in the visible and infrared,
99 respectively. Each data cube in the visible and/or infrared has a dimension of $432 \times N_s \times N_l$, where
100 432 is the number of spectral channels, N_l (number of lines) depends on the length of the
101 observation, while N_s (number of samples) is the number of spatial pixels composing a line, usually
102 equal to 256. The field of view of each square-shaped pixel is 0.25 mrad wide, hence a 256 pixel ×
103 256 pixel image, obtained by using a scanning mirror, covers a 64 mrad × 64 mrad field (which

corresponds to 220 arcmin × 220 arcmin). The full FOV is acquired in time by repeating successive acquisitions while the internal steerable mirror performs a scan or maintain it at fixed position while the spacecraft is drifting (pushbroom mode). The Earth data discussed here were acquired in the scan mode, allowing one to acquire a sequence of limbs consecutively.

The two VIRTIS-M focal planes are equipped with order-sorting filters to reduce contaminations due to higher spectral orders coming from the diffraction gratings. The two filters placed on the visible channel's detector have a junction placed at 0.640-0.651 μm; the five on the infrared channel detector have four junctions corresponding to 1.415-1.576 μm, 2.388-2.548 μm, 3.671-3.765 μm, and 4.284-4.397 μm wavelength [*Coradini et al.,* 2007]. In general the spectral radiance measured through the junctions has been corrected by the calibration pipeline. However, despite this correction some residual signals remain present on the first two junctions of the IR channel.

Since VIRTIS-M spectral range extends up to 5.1 μm, thermal environment plays a major role in the instrumental performance. During the fly-by, the VIRTIS radiator FOV was partially filled with the Earth, resulting in an optical bench temperature of about 147 K, significantly larger than the typical operative temperature of 135 K. This excess in temperature results in a wavelength shift of ~11 nm in the spectral calibration [*Migliorini et al.,* 2013], which was corrected in the calibration pipeline [*Filacchione et al.,* 2006].

In this paper we focus our analysis on data acquired in the IR spectral range, during the Earth gravity assist that occurred in November 2009. Prior to this fly-by, two more gravity assists with our planet had been performed by Rosetta on 4 March 2005 and between 13 and 14 November 2007. They will not be discussed here because the observations were not suitable to study nightglow emissions. During the first fly-by, no limb observation was performed, while during the second fly-by the limb mode observations concentrated on the dayside.

In the approach phase of the November 2009 Rosetta fly-by with the Earth, a sequence of full-disk images of the night side of the planet was acquired by VIRTIS-M from a distance spanning the

range 228,000-240,000 km. These data were not suitable for the O_2 and OH nightglow investigation because of the low spatial resolution, and hence are not considered in this study. When the spacecraft was less than 55,000 km away from the Earth, limb scans of the night side were carried out, starting from 150 km above the surface. These data satisfy our requirements to study the nightglow emission; the resulting vertical resolution (13 - 15 km/pixel) is similar to the thickness of the emission layer and the duration of each scan (2 min) is short enough to minimize possible time variability of the emissions.

The VIRTIS airglow data (image name I1_00216713355) consist of a collection of two limb scans in the same image, acquired a few minutes apart. The total duration of the IR channel scan is 12 minutes, corresponding to a sequence of 73 lines with an integration time of 7 sec each. The two limbs cover the latitude region from 38° to 47° in the northern hemisphere, and are centered at 1:30–2:00 AM solar local time. A more detailed description of the Earth's observations with VIRTIS was given in *Migliorini et al.* [2013] and *Hurley et al.* [2014].

In order to remove high frequency spatial noise, the cube-image was cleaned using a median filter combined with a smoothing procedure, applied in the spatial direction while the temporal and spectral dimensions were kept unchanged.

Since it was verified that the emission is roughly located at about 90 km, we averaged spectra collected between 87 and 105 km in order to increase the signal-to-noise ratio. A total of 300 individual spectra were summed together for each limb scan. The analysis was applied to the two VIRTIS observations separately, because the contribution of the background is different from one scan to the other. The radiance was converted into Rayleigh units (1 R corresponds to 10^6 photons/cm^2 s^{-1} in 4π steradians). The resulting spectrum is shown in Figure 1 for one of the two limb scans.

[HERE FIGURE 1]

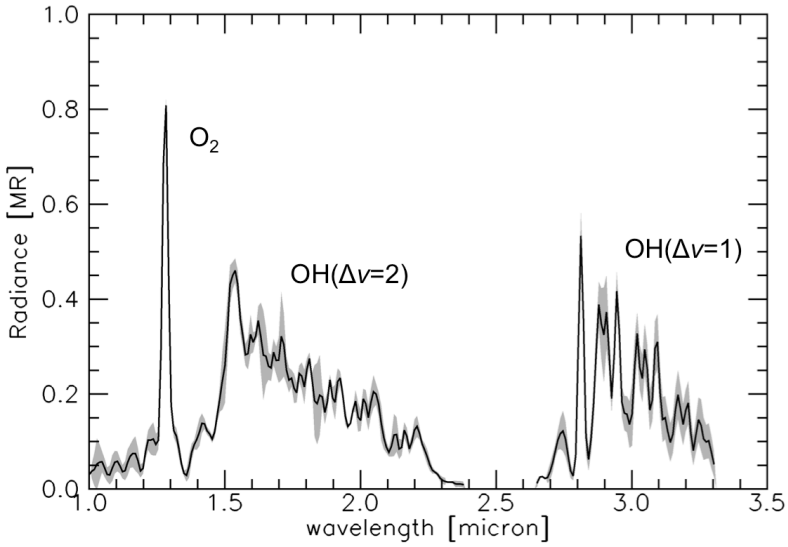

Figure1. *VIRTIS mean nightglow spectral radiance, in the altitude range 87-105 km. This dataset was processed with a median filter applied to the spatial component, in order to eliminate instrumental artifacts and with a background correction obtained by subtracting the spectrum measured between 120 and 125 km. Finally a wavelength calibration adjustment has been performed by applying a shift of ~11 nm towards shorter wavelengths (see also Migliorini et al. [2013]). The shaded area indicates the experimental error, calculated from the Noise Equivalent Spectral Radiance (NESR). The O_2 and OH(Δv=1,2) emissions are indicated.*

In the mean spectrum, the O_2 emission centred at 1.27 μm is clearly observed, as well as the Δ*v*=2 OH Meinel bands in the 1.4-2.4 μm region, and Δ*v*=1 bands in the 2.7-3.3 μm region, as indicated in Figure 1. The spectral region beyond 3.5 μm is dominated by the thermal emission and will not be discussed here.

Due to the limited spectral and spatial resolution, the variation of the peak emission's altitude for the different transitions studied by several authors [*Kaufmann et al.,* 2008; *McDade,* 1991; *von Savigny et al.,* 2012] cannot be verified in VIRTIS data.

3. Spectral model

We use the PGOPHER code (http://pgopher.chm.bris.ac.uk) to generate the line intensities of the rotational transitions for each vibrational band. The population distribution of the rotational levels is assumed to be Maxwellian. A rotational temperature of 200 K has been used in order to calculate a synthetic spectrum of the OH(Δv=1 and 2) emissions. This temperature is close to the average value at the mesopause [*Xu et al.,* 2012]. The variation of the rotational temperature with the vibrational levels has been discussed in *Cosby and Slanger* [2007] and *Noll et al.* [2014]. The difference between the rotational temperature in the v=1 manifold with respect to the v=10 manifold may be as large as 20 K. We simulated the rotational manifold for three different temperatures (200 K, 250 K and 300 K) and compared the simulations, convolved to the VIRTIS spectral resolution of 20 nm, with the observed spectra. It appeared that a rotational temperature of 200 K produced the best agreement. We note, however, that a rotational temperature difference of the order of 15-20 K only affects the structure inside each band, whose effect is negligible at the VIRTIS resolution. The emission spectra of the OH Meinel bands can thus be simulated by multiplying the calculated rotational manifolds for all vibrational quantum numbers (v=1-9) with the (unknown) populations of the upper levels and the relative Einstein coefficients for each vibrational transition. The Einstein coefficients were taken from *Xu et al.* [2012], calculated for a temperature of 200 K. The variation of the Einstein coefficients with temperature is very small (see e.g. *Xu et al.* [2012]) and thus our simulation is largely independent from the rotational temperature assumed. We then performed a least squares fit, which yielded the relative populations of the vibrational levels (v=1 to 9), taking into account both Δv=1 and Δv=2 bands. Figure 2 a-b shows the comparison between the VIRTIS spectra and the corresponding best fit for the available data.

[HERE FIGURE 2]

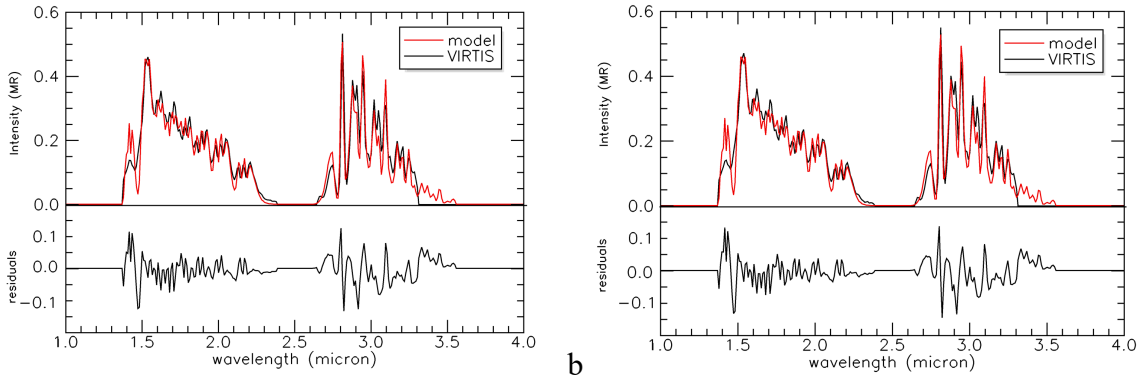

Figure 2. *a - Comparison between the VIRTIS spectrum (in black) and the spectral model (in red) for the first limb scan. The radiance outside the wavelengths regions covered by the OH emissions is set to 0, to limit the fit to the spectral region involving OH emissions. In the bottom panel of the figure, the residuals are shown. b- the same for the second limb scan.*

Similarly, a fit is obtained for the second VIRTIS spectrum, acquired within a few minutes from the first one. Both fits are in good agreement and provide consistent results for the populations of levels from v=1 to 9, except for the region between 1.4 and 1.5 µm, where a VIRTIS order-sorting filter junction is located. The model overestimates the intensity of the (2-0) transition at 1.46 µm in both spectra. The same discrepancy was observed by comparing the TIMED/SABER observations with models, as reported by *Xu et al.* [2012]. The TIMED/SABER observations had been corrected for the atmospheric attenuation, mostly due by water vapor. The good agreement between fit and VIRTIS observations of the (2-1) transition (around 2.82 µm) seems to exclude a specific quenching of the v=2 level. A possible explanation may be an error in the Einstein coefficient.

The average values of each population obtained for the two fits are provided in Table 1. To calculate the error in the vibrational populations, a set of 40 spectra was statistically generated by adding a random error to the original spectra. Each spectrum so obtained was fitted in the same way as the VIRTIS spectra, and the standard deviation of the results was taken as errors in the

217 determination of the vibrational population. Values of the percentage into each *v* level for the two
218 spectra, together with the calculated statistical error, are shown in Table 1.
219
220 **Table 1.** *The fitted OH vibrational population from the two VIRTIS spectra. The population values*
221 *are given in terms of percentage, while the errors are absolute.*
222

Level	Population – 1st fit	Error	Population – 2nd fit	Error
1	37.8	1.0	37.58	1.03
2	21.02	1.15	20.33	1.19
3	17.95	0.8	18.36	0.83
4	7.27	0.46	7.40	0.48
5	4.88	0.30	4.92	0.31
6	3.59	0.26	3.66	0.27
7	2.91	0.21	2.99	0.22
8	2.77	0.20	2.84	0.20
9	1.83	0.24	1.91	0.25

223
224 **4. Discussion**

225 The terrestrial nightglow emissions at the mid-latitudes of the northern hemisphere have been
226 investigated by using VIRTIS observations during a Rosetta Earth fly-by. During the season
227 (November) of these observations, the OH nightglow is quite intense at the altitudes, local time and
228 latitudes observed by VIRTIS, as reported also by the Wind Imaging Interferometer (WINDII) [*Liu*
229 *et al.,* 2008].

230 The vibrationally excited hydroxyl radical can decay through spontaneous emission of a photon,
231 giving rise to the observed emission, or can be quenched through collisions with other ambient
232 molecules (N_2, O_2) or atoms (O). The quenching process can occur stepwise involving transitions
233 from a specific vibrational level to a lower vibrational level, or all at once to the vibrational ground
234 level. This so-called sudden death mechanism, which can occur by vibrational quenching or by
235 chemical reaction, results in a smaller population of the low vibrational levels. While the radiative

processes depend merely on the Einstein coefficients, which are rather independent of temperature, the quenching processes may depend on the reaction rates, which may have strong temperature dependence and on the availability of quenchers. This implies that the vibrational population of the OH radical also may depends on the time and latitude of observation.

We compare our results with ground based measurements reported in *Krassovsky et al.* [1962], *Ferguson and Parkinson* [1963], *Harrison and Kendall* [1973], *Turnbull and Lowe* [1983], *Oliva and Origlia* [1992], and with model calculations by *Llewellyn et al.* [1978], *von Clarmann et al* [2010] and *Xu et al* [2012].

The heterogeneity of the previous measurements limits the comparison to few levels, which are present in all the considered datasets. For this reason, the comparison is made by normalizing all relative populations to that of the v=4 level, which has been reported by all authors.

Oliva and Origlia [1992] provide a list of high resolved rotational lines of hydroxyl, from which we derived the vibrational populations, by summing the identified lines for each level. As stated also by the authors, the line list is sometimes incomplete or limited by experimental issues, such as the atmospheric attenuation, so that the calculated populations have to be considered as lower limits.

The model proposed by *von Clarmann et al.* [2010] produces excited OH in all vibrational levels (v=1-10), by the hydrogen-ozone reaction. They used the non-LTE GRANADA model [*Funke et al.,* 2012] to calculate the relative OH populations for vibrational levels 0 to 9, for six different atmospheric conditions, assuming a stepwise quenching by O_2, N_2 and O. The model case describing a 'mid-latitudes night' atmosphere is the only one close to the observing conditions of the VIRTIS data discussed here. Hence, in Table 2 we report von Clarmann's results only for this model conditions. Note that the rate coefficients for OH production and for the quenching processes were much different from those used by *Llewellyn et al.* [1978].

Xu et al. [2012] compare the TIMED/SABER observations at 1.6 and 2.0 μm with a nightglow emission model, which cover 4 OH transitions out of the Δv=2. They concluded that reaction (a) is the dominant source for the OH nightglow emission for the vibrational levels with $v \geq 4$. The assumption of multi-quantum relaxation by O_2 and single-quantum relaxation by N_2 produced the best agreement with the SABER data, while the sudden death model did not reproduce the observations.

Except for our high v=3 population, all the relative populations from *Krassovsky et al.* [1962], *Harrison and Kendall* [1973] and *Ferguson and Parkinson* [1963] are in agreement with those derived here. We examined the possibility that the order-sorting filter at 1.415-1.576 μm could cause some residual instrumental effect (see e.g. *Tosi et al.,* 2012), but repeating the fits without this spectral interval did not produce appreciable changes in the results. The studies of *Krassovsky et al.* [1962] and *Harrison and Kendall* [1973] were based on observations of the Δv=3, 4, 5, 6 and the Δv=2, 3, 4, 5 sequences, but no information about the v=1 level could be obtained. Our analysis yields a population for the v=1 level which is about 5 times higher than the v=4 level. None of the previous analyses of experimental observations allowed the determination of the population of the v=1 level, while only two of them report the population of v=2. Of these two, the value of *Turnbull and Lowe* [1983] is very similar to ours, while those reported by *Oliva and Origlia* [1992] seem unrealistic. The population of v=1 level has been calculated by using different model simulations. *Llewellyn et al.* [1978] report a value 4.16 for the v=1 population with respect to the v=4 population, while *Xu et al.* [2012] report a value of 4.47, which is in reasonable agreement with the one obtained from the VIRTIS data. The value by *von Clarmann et al.* [2010] is significantly lower (3.27). The populations of levels 1 to 3 are underestimated in *von Clarmann et al.* [2010], while those with v>4 are higher than the populations derived from the VIRTIS/Rosetta data. These discrepancies and the difference with the populations calculated by *Xu et al.* [2012] possibly stem from the use of a single quantum relaxation in collisions with O by *von Clarmann et al.*, whereas

285 other models assume sudden-death chemical loss, where the excited OH molecule is directly
286 deactivated to the v=0 ground level. Another difference lies in the treatment of collisions with O_2:
287 *von Clarmann et al.* assume single quantum relaxation, while *Xu et al.* adopt a multi-quantum
288 scheme.

289 *Bunn and Gush* [1972] also measured the Δv=1, 2 sequences using balloon-borne instruments.
290 They found relative populations to be P(v=1)/P(v=2)=2.26 and P(v=2)/P(v=3)=1.76. Our study
291 suggests ratios of 1.82(16) and 1.14(12), respectively. The populations calculated from the
292 intensities of sky emissions taken from *Oliva and Origlia* [1992] do not follow the trend of
293 decreasing populations with increasing levels. It appears that their v=2 and v=7 populations are
294 largely underestimated. In fact, these authors mention that some of the line intensities could be
295 underestimated by large factors as they lie in regions of low atmospheric transmission.

296 Observations with the same VIRTIS instrument on the European Venus Express mission
297 allowed discovering the OH infrared night airglow on the Venus nightside in 2007 [*Piccioni et al.,*
298 2008]. The OH airglow spectra on the two planets show some differences in the intensity
299 distribution of the different bands. For example, the relative intensities of the Δv=1 bands
300 originating from v'>2 levels are higher in the terrestrial spectrum than in the Venus case. This
301 difference is presumably linked to the much larger abundance of CO_2 in the Venus atmosphere. On
302 Venus (and presumably on Mars), CO_2 is the dominant quencher, while O_2 and O play the major
303 role on Earth to deactivate vibrationally excited OH. *Soret et al.* [2012] demonstrated that for
304 Venus, compared with these terrestrial results, the paradigm of single vibrational quantum collision
305 deactivation by CO_2 provides a much better agreement with both the spectral structure and the
306 observed total brightness than the "sudden death" model.

307

308 **Table 2:** *Comparison of relative vibrational populations with previous studies. Values are*
309 *normalized at v=4, for which all the considered works provide values.*

	This work	*Krassovsky et al.* [1962] [a]	*Ferguson and Parkinson* [1963][a]	*Harrison and Kendall* [1973][a]	*Turnbull and Lowe* [1983] [a]	*Oliva and Origlia* [1992] [a]	*Llewellyn et al.* [1978] [b]	*vonClarmann et al.* [2010] [b]	*Xu et al.* [2012][b]
	38-47°N	55-62°N	55-62°N	56°N	43°N	29°S	45°N	Mid Lats	30-50°N
Level	*Nov 2009*	*1957-1958*	*1957-1958*	*Dec 1971*	*Apr 1980*	*Apr 1991*			
1	5.1±0.5						4.16	3.27	4.47
2	2.8±0.36				2.83	0.47	2.24	1.85	2.41
3	2.47±0.29	1.73	1.96	1.27	1.76	1.44	1.43	1.31	1.50
4	1.00±0.14	1.00	1.00	1.00	1.00	1.00	1.00	1.00	1.00
5	0.67±0.09	0.67	0.80	0.57		0.77	0.78	0.77	0.68
6	0.49±0.07	0.40	0.47	0.44	0.25	0.26	0.60	0.59	0.47
7	0.40±0.06	0.29	0.38	0.27	0.17	0.01	0.52	0.49	0.35
8	0.38±0.05	0.23	0.24	0.29	0.16	0.26	0.52	0.33	0.30
9	0.25±0.05	0.18	0.22	0.17	0.16	0.22	0.51	0.19	0.22

310 [a]Ground-based observations

311 [b]Numerical model

312

313 ## 5. Conclusions

314 For the first time, the data analyzed in this study allow investigating the OH infrared nightglow
315 emission from space and the vibrational population down to v =1. The Δv=1 and Δv=2 sequences
316 have been observed simultaneously. We remind, however, that VIRTIS spatial and spectral
317 resolution does not allow a complete retrieval of the vertical profile of each single transition, and
318 hence our measurements are limited. No correction for the telluric absorption is needed and the
319 populations deduced for the 1 to 9 vibrational levels might thus be considered as quite reliable.

320 The results of our analysis have been compared with ground-based observations and theoretical
321 models. A rather good agreement is found with the model proposed by *Xu et al.* [2012], assuming
322 multi-quantum relaxation by O_2 and single-quantum relaxation by N_2. The slightly smaller

populations for the levels v=1-3 in *Xu et al.* [2012] can possibly be explained by the omission of reaction (b) in their calculation.

Acknowledgments

The authors wish to thank ESA, ASI and the national space agencies supporting the Rosetta mission (Grant: ASI-INAF I/024/12/0). L. Soret and J.-C. Gérard are supported by the PRODEX program managed by ESA with the help of the Belgian Federal Space Science Policy Office.

The authors thank Dr. Xu and Dr. von Clarmann for kindly providing numerical values from their previous works.

333 **References**

334

335 Baker, D. J., and A. T. Jr. Stair (1988), Rocket measurements of the altitude distributions of the
336 hydroxyl airglow, *Physica Scripta*, 37, 611-622, doi: 10.1088/0031-8949/37/4/021.

337

338 Bates, D. R. and M. Nicolet (1950), The photochemistry of atmospheric water vapor, *J.*
339 *Geophys. Res.*, 55, 301-327, doi: 10.1029/JZ055i003p00301.

340

341 Bunn, F. E., and H. P. Gush (1972), Spectrum of the airglow between 3 and 4 Microns, *Can. J.*
342 *Phys.,* 50, 213-215, doi:10.1139/p72-033.

343

344 Coradini, A., et al. (2007), Virtis: An imaging Spectrometer for the Rosetta Mission, *Space Sci.*
345 *Rev.*, 128, 529-559, doi: 10.1007/s11214-006-9127-5.

346

347 Coradini, A., et al. (2010), Martian atmosphere as observed by VIRTIS-M on Rosetta
348 spacecraft, *J. Geophys. Res.*, 115, doi: 10.1029/2009JE003345.

349

350 Coradini, A., et al. (2011), The surface composition and temperature of Asteroid 21 Lutetia as
351 observed by Rosetta/VIRTIS, *Science*, 334, 492-494, doi: 10.1126/science.1204062.

352

353 Cosby P. C. and T. G. Slanger (2007), OH spectroscopy and chemistry investigated with
354 astronomical sky spectra, *Can. J. Phys.*, 85, 77-99.

355

356 Ferguson, A. F., and D. Parkinson (1963), The hydroxyl bands in the nightglow, *Planet. Space*
357 *Sci.*, 11, 149-159, doi: 10.1016/0032-0633(63)90136-3.

358

359 Filacchione G. et al. (2006), On-ground characterization of Rosetta/VIRTIS-M. II. Spatial and
360 radiometric calibrations, *Rev. Sci. Instrum.*, 77, 103-106.
361
362 Funke, B., M. López-Puertas, M. García-Comas, M. Kaufmann, M. Höpfner, and G. P. Stiller
363 (2012), GRANADA: A Generic RAdiative transfer AnD non-LTE population algorithm, *J. Quant.*
364 *Spectrosc. Radiat. Transfer*, 113(14), 1771-1817, 2012.
365
366 Gao, H., J. Xu, Q. Wu (2010), Seasonal and QBO variations in the OH nightglow emission
367 observed by TIMED/SABER, *J. Geophys. Res.,* 115, A06313, doi:10.1029/JA014641.
368
369 Harrison, A. W., and D. J. W. Kendall (1973), Airglow hydroxyl intensity measurements 0.6–
370 2.3 μm, *Planet. Space Sci.*, 21, 1731–1741,doi:10.1016/0032-0633(73)90164-5.
371
372 Hurley J., P. G. J. Irwin, A. Adriani, M. Moriconi, F. Oliva, F. Capaccioni, A. Smith, G.
373 Filacchione, F. Tosi, G. Thomas (2014), Analysis of Rosetta/VIRTIS spectra of earth using
374 observations from ENVISAT/AATSR, TERRA/MODIS and ENVISAT/SCIAMACHY, and
375 radiative-transfer simulations, *Planet. Space Sci.*, 90, p. 37-59, doi: 10.1016/j.pss.2013.06.012.
376
377 Kaufmann, M., C. Lehmann, L. Hoffmann, B. Funke, M. López-Puertas, C. v. Savigny, M.
378 Riese (2008), Chemical heating rates derived from SCIAMACHY vibrationally excited OH limb
379 emission spectra, *Adv. Space Res.*, 41, 1914-1920, doi: 10.1016/j.asr.2007.07.045.
380
381 Krassovsky, V. I., N. N. Shefov, and V. I. Yarin (1962), Atlas of the airglow spectrum 3000-
382 12400 Å, *Planet. Space Sci.*, 9, 883, doi: 10.1016/0032-0633(62)90008-9.
383
384

385 Leyrat, C., A. Coradini, E. Erard, F. Capaccioni, M. T. Capria, P. Drossart, M. C. De Sanctis, F.
386 Tosi, and the Rosetta/VIRTIS Team (2011), Thermal properties of the asteroid (2867) Steins as
387 observed by VIRTIS/Rosetta. *Astron. Astrophys.* 531, id.A168, doi: 10.1051/0004-
388 6361:201116529.
389
390 Llewellyn, E. J., B. H. Long and B. H. Solheim (1978), The quenching of OH* in the
391 atmosphere, *Planet. Space Sci.*, 26, 525–531, doi:10.1016/0032-0633(78)90043-0.
392
393 Liu, G., G. G. Shepherd, R. G. Roble (2008), Seasonal variations of the nighttime O(1S) and
394 OH airglow emission rates at mid-to-high latitudes in the context of the large-scale circulation. *J.*
395 *Geophys. Res,* 113, doi: 10.1029/2007JA012854.
396
397 Lowe, R. P., L. M. Leblanc, K. L. Gilbert (1996), WINDII/UARS observation of twilight
398 behavior of the hydroxyl airglow, at mid-latitude equinox, *J. Atmos. Terr. Phys.* 58, 1863–1896,
399 doi:10.1016/0021-9169(95)00178-6. ~~1996JATP...58.1863L.~~
400
401 McDade, I. C. (1991), The altitude dependence of the OH($X^2\Pi$) vibrational distribution in the
402 nightglow: some model expectations. *Planet. Space Sci.* 39, 1049–1057, doi: 10.1016/0032-
403 0633(91)90112-N.
404
405 Mélen, F., A. J. Sauval, N. Grevesse, C. B. Farmer, Ch. Servais, L. Delbouille, G. Roland
406 (1995), A new analysis of the OH radical spectrum from Solar Infrared observations. *J. Mol. Spec.,*
407 174, 490-509.
408

409 Melo, S. M. L., R. P. Lowe, and H. Takahashi (1999), The nocturnal behaviour of the hydroxyl
410 airglow at the equatorial and low latitudes as observed by WINDII: Comparison with ground-based
411 measurements, *J. Geophys. Res., 104,* 24,657-24,665, doi:10.1029/1999JA900291.
412
413 Meriwether, J. W. (1989), A review of the photochemistry of selected nightglow emissions from
414 the mesopause. *J. Geophys. Res.*, 94, 14629-14646.
415
416 Migliorini, A., et al. (2013), Comparative analysis of airglow emissions in terrestrial planets,
417 observed with VIRTIS-M instruments on board Rosetta and Venus Express, *Icarus*, 226, 1115-
418 1127, doi: 10.1016/j.icarus.2013.07.027.
419
420 Noll S., et al. (2014), OH populations and temperatures from 25 bands, *ACPD*, 14, 32979-
421 33043.
422
423 Oliva, E., and L. Origlia (1992), The OH airglow spectrum: a calibration source for infrared
424 spectrometers, *Astron. Astrophys.*, 254, 466-471.
425
426 Piccioni, G., et al. (2008), First detection of hydroxyl in the atmosphere of Venus, *Astron.*
427 *Astrophys.* 483, L29-L33, doi: 10.1051/0004-6361:200809761.
428
429 Russell, J. P., W. E. Ward, R. P. Lowe, R. G. Roble, G. G. Shepherd, and B. Solheim (2005),
430 Atomic oxygen profiles (80 to 115 km) derived from Wind Imaging Interferometer/Upper
431 Atmospheric Research Satellite measurements of the hydroxyl and green line airglow: Local time-
432 altitude dependence, *J. Geophys. Res., 110*, D15305, doi:10.1029/2004JD005570.
433

Schulz, R. (2009), Rosetta – One comet rendezvous and two asteroids fly-bys,. *Solar Syst. Res.,* 43, 343–352, doi: 10.1134/S0038094609040091.

She, C. Y., R. P. Lowe (1998), Seasonal temperature variations in the mesospause region at mid-latitude: comparison of lidar and hydroxyl rotational temperatures using WINDII/UARS heights profiles, *J. Atmos. Sol.-Terr. Phys.,* 60, 1573–1583, doi: 10.1016/S1364-6826(98)00082-0.

Shepherd, G. G., R. Roble, S. P. Zhang, C. McLandress, and R. Wiens (1998), Tidal influence on midlatitude airglow: Comparison of satellite and ground-based observations with TIME-GCM predictions, *J. Geophys. Res.,* 103, 14,741-14,751, doi:10.1029/98JA00884.

Snively, J. B., V. P. Pasko, and M. J. Taylor (2010), OH and OI airglow layer modulation by ducted short-period gravity waves: Effects of trapping altitude, *J. Geophys. Res.,* 115, A11311, doi:10.1029/2009JA015236.

Soret, L., J. C. Gérard, G. Piccioni, P. Drossart (2012), The OH Venus nightglow spectrum: Intensity and vibrational composition from VIRTIS-Venus Express observations, *Icarus,* 73, 387-396, http://dx.doi.org/10.1016/j.pss.2012.07.027.

Tosi, F. et al. (2010), The light curve of Asteroid 2867 Steins measured by VIRTIS-M during the Rosetta fly-by, *Planet. Space Sci.* 58, 1066–1076, doi: 10.1016/j.pss.2010.03.019.

Tosi, F. et al. (2012), The light curve of Asteroid 21 Lutetia measured by VIRTIS-M during the Rosetta fly-by, *Planet. Space Sci.* 66, 9–22, doi: 10.1016/j.pss.2011.11.016.

459 Turnbull, D. N., and R. P. Lowe (1983), Vibrational population distribution in the hydroxyl
460 night airglow, *Can. J. Phys.*, 61, 244–250, doi:10.1139/p83-033.
461
462 von Clarmann, T., et al. (2010), Do vibrationally excited OH molecules affect middle and upper
463 atmospheric chemistry?, *Atmos. Chem. Phys.,* 10, 9953-9964, doi: 10.5194/acp-10-9953-2010.
464
465 von Savigny, C., I. C. McDade, K. U. Eichmann, and J. P. Burrows (2012), On the dependence
466 of the OH Meinel emission altitude on vibrational level: SCIAMACHY observations and model
467 simulations, *Atmos. Chem. Phys.,* 12, 8813–8828, doi:10.5194/acp-12-8813-2012.
468
469 von Savigny, C., and O. Lednyts'kyy (2013), On the relationship between atomic oxygen and
470 vertical shifts between OH Meinel bands originating from different vibrational levels, *Geophys.*
471 *Res. Lett.*, 40, 5821-5825, doi:10.1002/2013GL058017.
472
473 Ward, W. E. (1999), A simple model of diurnal variations in the mesospheric oxygen
474 nightglow, *Geophys. Res. Lett., 26*, 3565-3568, doi:10.1029/1999GL003661.
475
476 Xu, J., A. K. Smith, G. Jiang, H. Gao, Y. Wei, M. G. Mlynczak (2010), Strong longitudinal
477 variations in the OH nightglow, *Geophys. Res. Lett.*, 37, L21801, doi:10.1029/2010GL043972.
478
479 Xu, J., H. Gao, A. K. Smith, Y. Zhu (2012), Using TIMED/SABER nightglow observations to
480 investigate hydroxyl emission mechanisms in the mesopause region, *J. Geophys. Res.,* 117,
481 D02301, doi:10.1029/2011JD016342.
482

Zhang, S. P., and G. G. Shepherd (1999), The influence of the diurnal tide on the O(^{1}S) and OH emission rates observed by WINDII on UARS, *Geophys. Res. Lett.* 26, 529-532, doi:10.1029/1999GL900033.

Zhang, S. P., R. Wiens, B. Solheim, and G. Shepherd (1998), Nightglow zenith emission rate variations in the O(^{1}S) at low latitudes from wind imaging interferometer (WINDII), *J. Geophys. Res., 103*, 6251-6259, doi:10.1029/97JD03326.

Zhao, Y., M. J. Taylor, X. Chu (2005), Comparison of simultaneous Na lidar and mesospheric nightglow temperature measurements and the effects of tides on the emission layer heights, *J. Geophys. Res.,* 110, D09S07. doi:10.1029/2004JD005115